

Gas Cavities inside Dust Cavities in Disks Inferred from ALMA Observations

Nienke van der Marel¹, Ewine F. van Dishoeck^{1,2}, Simon Bruderer²,
Paola Pinilla¹, Tim van Kempen¹, Laura Perez³ and Andrea Isella⁴

¹ Leiden Observatory, Leiden, the Netherlands
email: nmarel@strw.leidenuniv.nl

² MPE, Garching bei Munchen, Germany

³ NRAO, Socorro, NM, USA

⁴ Rice University, Houston, TX, USA

Abstract. Protoplanetary disks with cavities in their dust distribution, also named transitional disks, are expected to be in the middle of active evolution and possibly planet formation. In recent years, millimeter-dust rings observed by ALMA have been suggested to have their origin in dust traps, caused by pressure bumps. One of the ways to generate these is by the presence of planets, which lower the gas density along their orbit and create pressure bumps at the edge. We present spatially resolved ALMA Cycle 0 and Cycle 1 observations of CO and CO isotopologues of several famous transitional disks. Gas is found to be present inside the dust cavities, but at a reduced level compared with the gas surface density profile of the outer disk. The dust and gas emission are quantified using the physical-chemical modeling code DALI. In the majority of these disks we find clear evidence for a drop in gas density of at least a factor of 10 inside the cavity, whereas the dust density drops by at least a factor 1000. The CO isotopologue observations reveal that the gas cavities are significantly smaller than the dust cavities. These gas structures suggest clearing by one or more planetary-mass companions.

Keywords. planetary systems: formation, planetary systems: protoplanetary disks, techniques: interferometric, molecular data, radiative transfer

1. Introduction

Planets are formed in disks of dust and gas surrounding young stars (Williams & Cieza 2011). Of particular interest are the so-called transitional disks with cleared out dust cavities. These disks are expected to be in the middle of active disk evolution and planet formation. Transition disks are generally identified by a dip in the mid infrared part of their SED due to the lack of hot dust (Espaillat *et al.* 2014). Several mechanisms can be responsible for the appearance of a dust cavity: grain growth (Dullemond & Dominik 2005), photoevaporation (Clarke *et al.* 2001), clearing by (sub)stellar or planetary companions (Lin & Papaloizou 1979) and instabilities at the edges of dead zones (Regály *et al.* 2012). The latter two scenarios include trapping of the millimeter-dust in ring-like or asymmetric structures. Dust trapping can happen in a local pressure bump in the outer part of the disk due to the interaction between gas and dust (Weidenschilling 1977) and has been suggested to explain the observed structures in transition disks (Pinilla *et al.* 2012, van der Marel *et al.* 2013).

In order to distinguish between the different mechanisms, it is essential to know the distribution of dust *and* gas inside the dust cavity: in case of grain growth, both millimeter dust and gas will remain as in a full disk (Birnstiel *et al.* 2010); photoevaporation will clear the gas and dust simultaneously from the inside out; dead zones will only remove the dust by trapping, the gas density remains the same inside the cavity; a companion

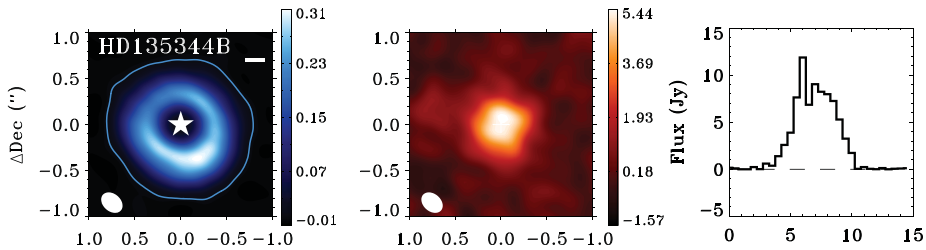


Figure 1. ALMA observations of the 690 GHz dust continuum and ^{12}CO 6-5 line of HD135344B, one of six targets in the sample of the ^{12}CO study in van der Marel et al. (2015a). In the images, the beam is indicated in the lower left corner. **Left:** Continuum image. The white bar in the upper right corner indicates the 30 AU scale and the yellow contour gives the 3σ detection limit. **Center:** zero-moment ^{12}CO map. **Right:** ^{12}CO spectrum integrated over the entire disk. The dashed line indicates the zero flux level.

will lower the gas density inside the dust cavity. In contrast to scattered light images at optical wavelengths, CO millimeter lines can actually quantify the gas density structure.

ALMA (Atacama Large Millimeter/submillimeter Array) allows us to zoom in and resolve the cavities in the gas and dust in transition disks, through dust continuum and CO line observations. We present a sample study of 6 transition disks that have been observed in ALMA Cycle 0 at subarcsecond resolution in continuum and ^{12}CO . Five disks were observed in Band 9 (690 GHz or 450 μm), one disk in Band 7 (345 GHz or 850 μm).

2. Results

2.1. Observations

The sample consists of SR21, HD135344B, LkCa15, SR24S and RXJ1615-3255 (observed in Band 9 or 690 GHz, partially presented in Perez *et al.* 2014) and J1604-2130 (observed in Band 7 or 345 GHz, first presented in Zhang *et al.* 2014). One example of the disk observations in continuum and integrated ^{12}CO emission is shown in Figure 1, the others are presented in van der Marel et al. (2015a).

This Figure shows that ^{12}CO emission peaks inside the dust cavity, indicating that there is still gas inside the cavity. In Figure 2 the intensity cuts (cuts along the major axis for the integrated CO and continuum emission) for all six targets are presented. It is clear that all targets show gas inside the dust cavity. However, as ^{12}CO emission is optically thick, these images do not give direct information on the gas density distribution.

2.2. Modeling

In order to quantify the gas and dust distribution, radiative transfer modeling is required. We use DALI, a full physical-chemical modeling code, to analyze the emission (Bruderer 2013). DALI solves for the dust temperatures through continuum radiative transfer, starting from a given surface density profile (Figure 3). Subsequently, DALI calculates the chemical abundances, the molecular excitation and the thermal balance of the gas, where effects such as photodissociation, freeze-out, decoupling of gas and dust temperature and UV heating are included, and finally raytraces images and spectra.

For the modeling, the dust surface density is constrained first by fitting a parameterized model with an empty dust cavity to the SED, the millimeter continuum image and the

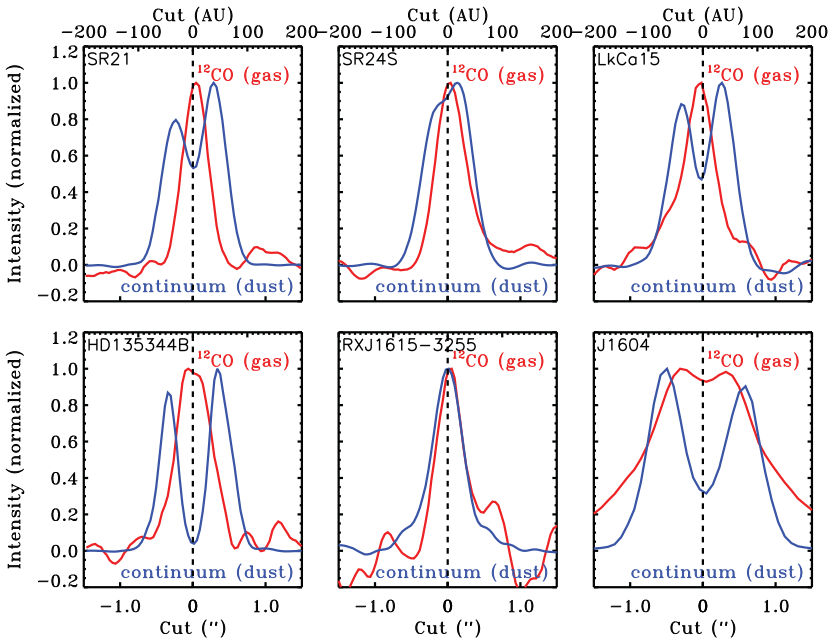


Figure 2. Normalized intensity cuts along the major axis of the continuum emission and the integrated ^{12}CO map of each disk in the sample. The continuum is indicated in blue, the integrated ^{12}CO in red. The cuts reveal that the ^{12}CO emission is peaking inside the dust cavity.

millimeter visibilities. The latter provides the best constraints on the dust cavity size r_{cav} . Next, the drop in dust density inside the cavity is constrained by changing δ_{dustcav} . For all disks it was found that δ_{dustcav} is 10^{-3} or less, implying a dust density drop of least a factor 1000.

Using the derived dust density profile, the gas density profile is computed by taking a gas-to-dust ratio of 100 in the outer disk, and setting δ_{gas} inside the cavity equal to 1, since the ^{12}CO emission peaks inside the cavity. The resulting images are compared with the observed ^{12}CO data, and it turns out that the model overpredicts the ^{12}CO emission. By lowering δ_{gas} by a factor 10–100 inside the cavity the emission is well reproduced for each of the six disks. The reason that optically thick ^{12}CO decreases with δ_{gas} is that the $\tau = 1$ surface shifts down, closer to the mid-plane when δ_{gas} is decreased. Due to the strong vertical temperature gradient the emission thus drops slightly with δ_{gas} as well (Bruderer 2013).

The different drops in density of the gas and dust inside the cavity directly points towards the companion clearing scenario for these disks, where the companion has cleared its orbit and traps the millimeter-sized dust at the edge, creating a millimeter continuum ring.

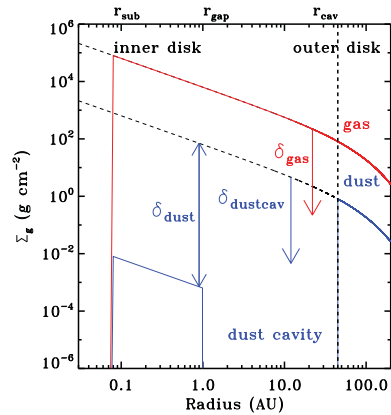


Figure 3. Generic surface density model of gas and dust that is used as input for DALI. Inside the cavity ($< r_{\text{cav}}$), the dust density drops by a factor δ_{dustcav} , the gas density by a factor δ_{gas} . The inner disk is reproduced by an additional δ_{dust} . The δ -values are free parameters in the model, after the outer disk density is matched to the data. Figure taken from van der Marel et al. (2015a).

2.3. New CO isotopologue data

Recently we have received ALMA Cycle 1 Band 7 data of CO isotopologues ^{13}CO and C^{18}O of 3 transition disks, including SR21 and HD135344B (van der Marel et al. 2015b). The data of HD135344B are presented in Figure 4. CO isotopologues are less optically thick and trace the density more directly than the ^{12}CO . The CO isotopologue images again show gas emission inside the dust cavity, but now also revealing a gas ring. The gas cavity radius is smaller than the dust cavity radius in all cases. This is consistent with the planet clearing scenario and trapping, as the dust is expected to be trapped further out than the planet orbit (Pinilla et al. 2012).

The previous models from the ^{12}CO study fit well with the isotopologue data, except that the cavity radius for the gas is now seen directly and found to be smaller than that of the dust. These new data will be presented in van der Marel et al. (2015b).

3. Conclusions

The ALMA CO observations of the transition disks observed so far show that gas is present inside the dust cavities. Analysis of the CO emission in the six transition disks in this recent study reveals that gas cavities have smaller drops in density than the millimeter-dust cavities. In addition, CO isotopologue data reveal gas cavities to be smaller in radius than the dust cavities. These findings strengthen the conclusion that embedded planets or companions are the main clearing mechanism. Ultimately, observations should be compared directly with the output of planet-disk interaction models, rather than parametrized models, to confirm the proposed scenario.

References

- Birnstiel, T., Dullemond, C. P., & Brauer, F. 2010, *A&A*, 513, A79
 Bruderer, S. 2013, *A&A*, 559, A46
 Clarke, C. J., Gendrin, A., & Sotomayor, M. 2001, *MNRAS*, 328, 485
 Dullemond, C. P. & Dominik, C. 2005, *A&A*, 434, 971
 Espaillat, C., Muzerolle, J., Najita, J., et al. 2014, in *Protostars and Planets VI*, p. 497
 Lin, D. N. C. & Papaloizou, J. 1979, *MNRAS*, 188, 191
 Pérez, L. M., Isella, A., Carpenter, J. M., & Chandler, C. J. 2014, *ApJL*, 783, L13
 Pinilla, P., Benisty, M., & Birnstiel, T. 2012, *A&A*, 545, A81
 Regály, Z., Juhász, A., Sándor, Z., & Dullemond, C. P. 2012, *MNRAS*, 419, 1701
 van der Marel, N., van Dishoeck E. F., Bruderer, S., et al. 2015, subm. to *A&A*,
 van der Marel, N., van Dishoeck, E., Bruderer, S., Perez, L., & Isella, A. 2015, *A&A*, 579, 106
 van der Marel, N., van Dishoeck, E. F., Bruderer, S., et al. 2013, *Science*, 340, 1199
 Weidenschilling, S. J. 1977, *MNRAS*, 180, 57
 Williams, J. P. & Cieza, L. A. 2011, *ARA&A*, 49, 67
 Zhang, K., Isella, A., Carpenter, J. M., & Blake, G. A. 2014, *ApJ*, 791, 42

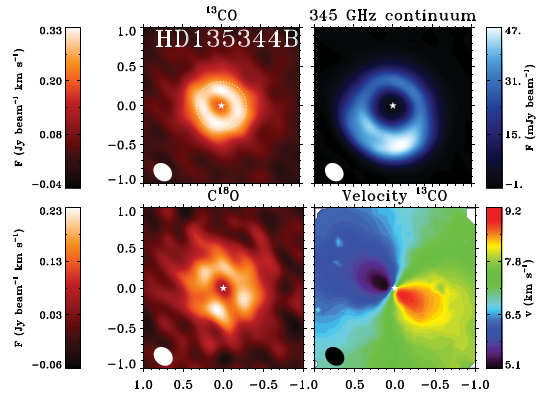


Figure 4. ALMA Cycle 1 observations of the continuum, ^{13}CO and C^{18}O 3-2 lines of HD135344B. **Top left:** zero-moment ^{13}CO map; **Top right:** Continuum map; **Bottom left:** zero-moment C^{18}O map; **Bottom right:** first moment ^{13}CO map.